JETIR.ORG ISSN: 2349-5162 | ESTD Year : 2014 | Monthly Issue
JOURNAL OF EMERGING TECHNOLOGIES AND INNOVATIVE RESEARCH (JETIR)
An International Scholarly Open Access, Peer-reviewed, Refereed Journal

Desalination via a Multistage Solar Still

Evangelene M, Bivin Joe A
Student, Student
St.Josephs college of Engineering, Chennai, India

Abstract : Seawater desalination is a promising solution to address global water scarcity, but current large-scale approaches are not suitable for developing regions. Previous studies on interfacial solar vapor generation showed limited efficiency. Recent progress in combining solar heating with vaporization enthalpy recycling improved desalination performance, but there is still room for improvement. In this work, a thermally-localized multistage solar still was developed, achieving ultra-high efficiency. The prototype device collected over 75% of vaporized water through condensation and demonstrated salt-rejection capabilities. The findings present potential for high-efficiency passive desalination and other solar thermal applications, offering a scalable and low-cost solution for clean water production in off-grid areas.

I. INTRODUCTION

Access to potable water is a fundamental human right and a prerequisite for sustainable development. However, with the increase in population, industrialization, and climate change impacts, water scarcity has become a critical issue faced by many regions worldwide. Desalination, the process of converting saline water into freshwater, has gained prominence as a potential solution to alleviate water scarcity. It harnesses the abundant source of seawater or brackish water, providing an alternative water resource. Solar desalination, specifically solar stills, has emerged as an attractive technology due to its simplicity, scalability, and utilization of renewable energy. Traditional solar stills utilize solar energy to evaporate water, leaving behind the dissolved salts, and subsequently condense the vapor to produce freshwater. While these systems have been successfully employed in various settings, they suffer from limited productivity and relatively low energy efficiency. Multistage solar stills comprise a series of interconnected still units, enabling improved water production rates and energy efficiency compared to single-stage designs. By capitalizing on the residual heat from the condensation process, multistage solar stills recycle energy and create a cascading effect that significantly enhances freshwater output. The objective of this paper is to present a comprehensive review of multistage solar still desalination technologies, highlighting their design principles, operational parameters, and performance metrics.

1.1 DESIGN

To optimize the performance of a multistage solar still, several design parameters, including device width (a), air gap thickness (b) of each unit stage, and the total number of stages (n), must be carefully considered. In this study, a unit stage height of 12 cm was chosen to align with the wicking length of the capillary wick, which has a thickness of 0.5 mm (Fig 1a). The thickness of the aluminum sheet is 0.5mm (Fig 1b). Determining suitable values for b and n involves evaluating heat and mass transport within each stage.

Decreasing the air gap thickness (b) can reduce vapor transport resistance but may lead to increased conduction loss through the gap. While this conduction loss can be utilized by the subsequent stage to promote evaporation, it reduces vapor generation at the previous higher-temperature stage, resulting in decreased overall solar-to-vapor conversion efficiency.

On the other hand, increasing the total number of stages (n) theoretically enhances overall performance. However, in practice, the benefits of adding more stages diminish once the total number becomes sufficiently large due to heat loss from the sidewall. The thickness of the aluminum sheet is 0.5mm (Fig 1b). The absorber sheet plays a crucial role in energy conversion, heat transfer, and substance capture processes, making it a vital component in various industries and applications. The aluminum sheet is painted with black paint for high heat absorption rate (Fig 1c).

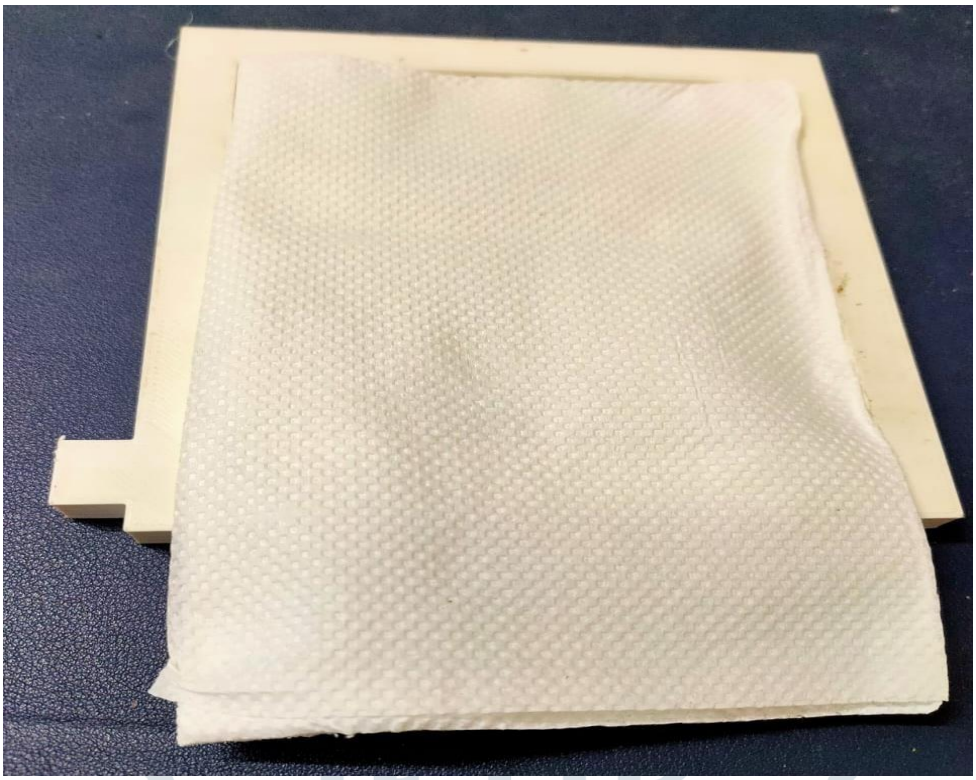

Fig 1a Capillary Wick

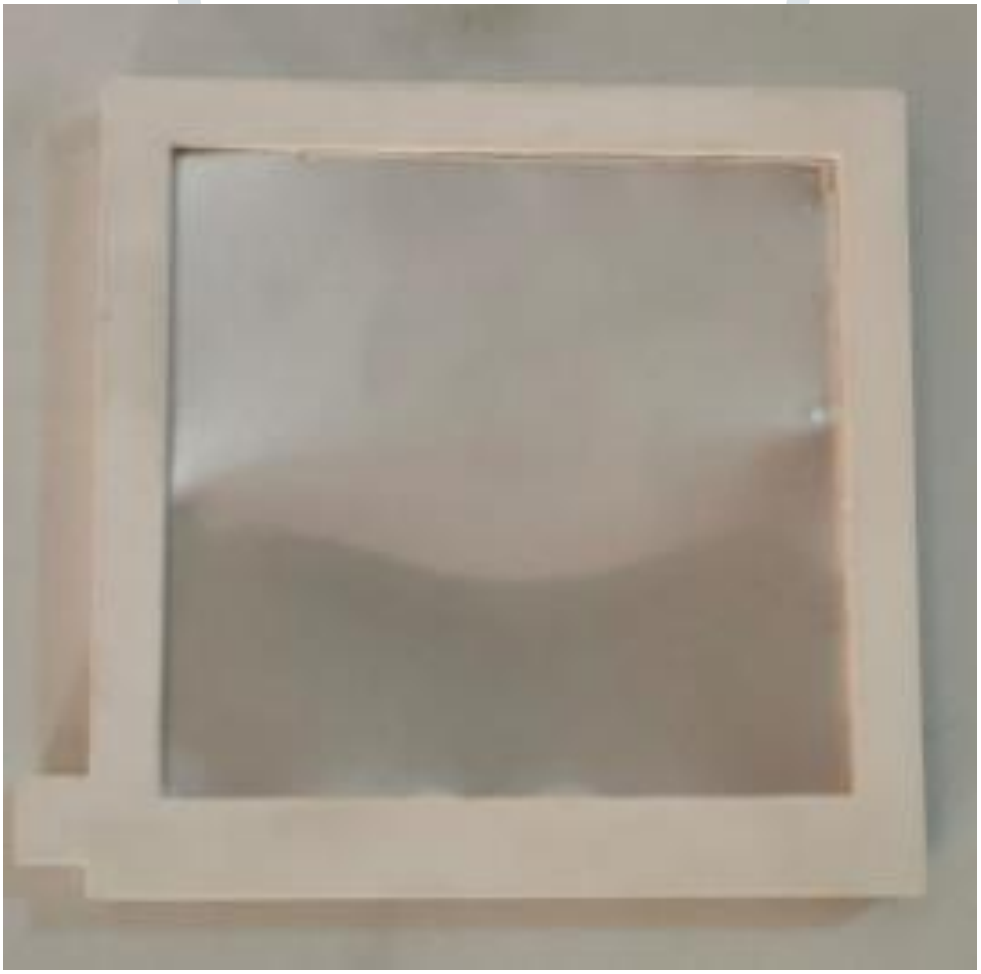

Fig 1b Aluminum sheet

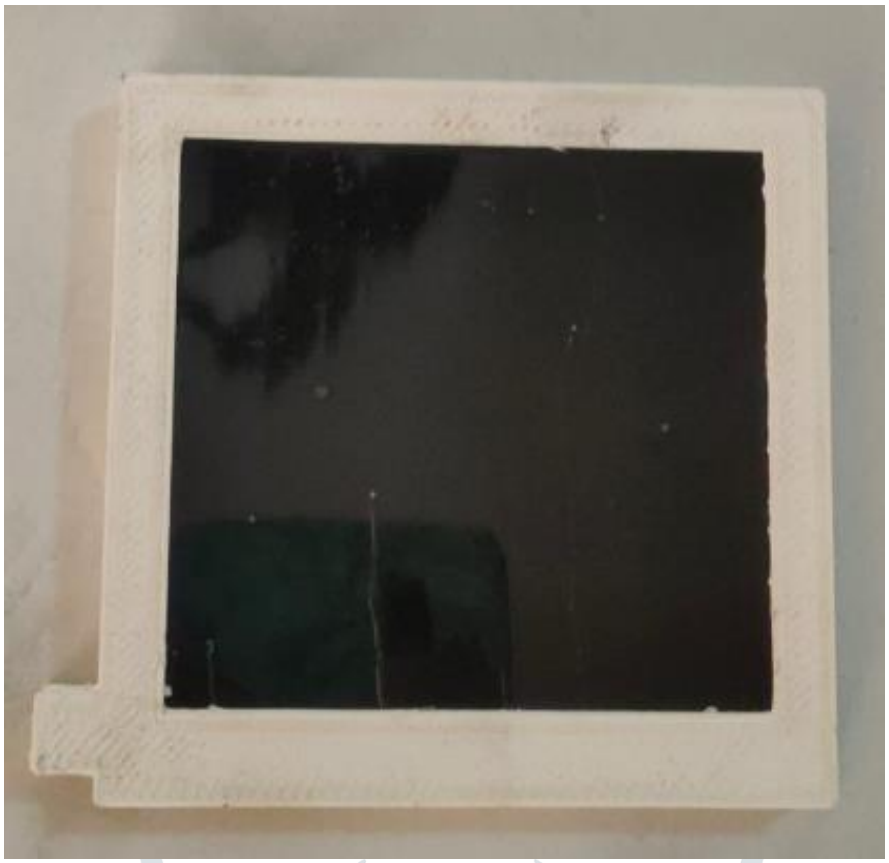

Fig 1c Absorber sheet

To ensure high solar-to-vapor conversion efficiency while avoiding excessive stages, the number of stages must be optimized. In this study, a theoretical model was developed that considers the coupled effects of heat and mass transport. The analysis revealed an optimized air gap thickness for a given device height. For the chosen device width (a = 12 cm), the optimal value of b was found to be approximately 6 mm. This configuration, with a = 12 cm and b = 6 mm, demonstrated negligible performance improvement with an increasing number of stages beyond approximately 20.
Considering practical considerations, a gap thickness of 6 mm (larger than the typical droplet size on the condenser) was selected to prevent contact between the condensate and the evaporator, enabling collection. For the proof-of-concept demonstration, a total of 10 stages (n = 10) were chosen to maintain a small and portable device size.
The chosen configuration (a = 12 cm, b = 6 mm, and n = 10) proved to be close to the optimal point, as determined by the theoretical analysis. It was found that effective sidewall thermal insulation is crucial for enhancing efficiency by preventing heat loss.

The prototype solar still utilized 3D-printed frames, benefitting from the integration of Programmable Logic Controllers (PLCs). PLA is a widely used 3D printing material known for its ease of use, biodegradability, and good print quality. Derived from renewable sources, it offers dimensional accuracy and comes in various colors. Ideal for prototyping and consumer products, PLA is eco-friendly and post-processing friendly. PLC integration in 3D printing enables precise control, automation, and improved print quality by regulating temperature, material flow, and movement, optimizing printing conditions (Fig 1d)

Fig 1d Experimental setup of 10 stage multilevel solar still

The prototype solar still consisted of a commercial solar absorber, a glass cover with an antireflection coating, and aluminum condensers. The capillary wick, with a thickness of 0.5 mm, was made from low-cost paper towels to facilitate efficient water transport. Hydrophobic coating on the materials enabled easy removal of condensed water through dropwise condensation. The transparency and absorptance properties of the materials were confirmed through spectrophotometer measurements.

The estimated material cost of the prototype, considering the 3D-printed frames, capillary wick, and other components, was approximately $1.54. Further cost reduction is possible by optimizing the design of the frames or exploring alternative, more affordable materials.

2.1 WORKING

The recent experimental demonstrations mainly focused on combining the benefits of multiple stages and heat localization to achieve a higher performance for solar desalination, the fundamental limits to the overall performance and the corresponding design strategies were not explored. Therefore, opportunities to further develop a low-cost and high-performance architecture were not demonstrated. To tackle this challenge, we performed analysis to obtain a fundamental understanding of heat and mass transport within the device, which leads to an optimized design approaching the theoretical limit. We also fabricated a ten-stage salt-accumulation-free solar still prototype using low-cost materials.

The first stage facing the incident sunlight consists of a layer of thermal insulation, a solar absorber, a capillary wick, and a condenser which are aligned along the direction of solar illumination (Fig. 2a). Each of the subsequent stages is composed of a capillary wick and a condenser separated by an air gap (Fig. 2b). The condenser of the last stage is inserted into the bulk brine to maintain its temperature close to the ambient environment, which ensures a large vapor pressure gradient across each stage.

The solar absorber, sandwiched between the glass layer and the first capillary wick, converts solar energy into heat. The glass suppresses heat losses from the solar absorber through conduction, convection, and radiation, due to its ultralow thermal conductivity and high infrared opacity. Thermal energy is transferred from the absorber to the capillary wick attached on the backside, where brine is driven up by capillarity and evaporates due to the elevated temperature. Vapor travels across the air gap between the evaporator and condenser, releasing thermal energy through condensation.

The condensed clean water at each stage is collected, while the released thermal energy is transferred to drive evaporation in the next stage (Fig. 2a and 2b), realizing enthalpy recycling. The solar still architecture enables high-performance desalination due to three key attributes that optimize heat and mass transport. First, vaporization enthalpy recycling is realized by the multistage configuration, where the latent heat released from the previous stage is harnessed by the next stage to induce evaporation.

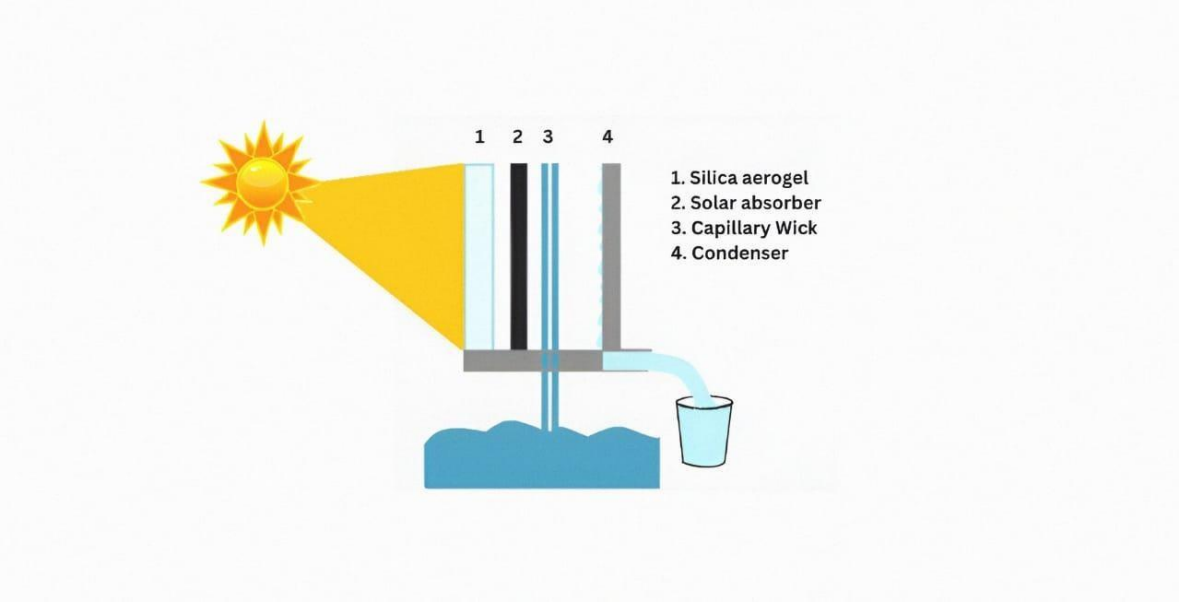

Fig. 2a Single stage solar still for desalination

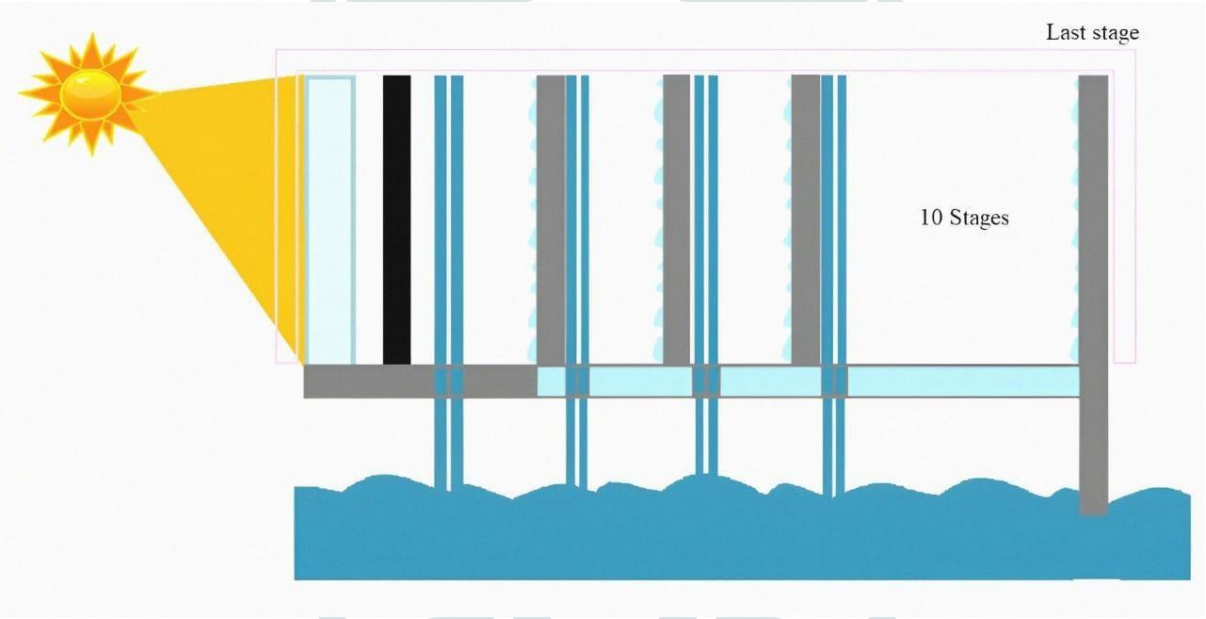

Fig. 2b multi-Stage solar still for desalination

Our experiments demonstrate that over 75% of the vaporized water can be collected through condensation, and the device can passively reject accumulated salt through diffusion during nighttime operation. The design principles and device architecture presented in this study have the potential to advance high-efficiency passive desalination technologies and other solar thermal applications. While recent experimental demonstrations have focused on combining multiple stages and heat localization to achieve improved performance in solar desalination, the fundamental limits of overall performance and corresponding design strategies have not been thoroughly explored. As a result, opportunities to develop a low-cost and high-performance architecture have not been adequately demonstrated. To address this challenge, we conducted an analysis to gain a fundamental understanding of heat and mass transport within the device. We fabricated a prototype of a ten-stage multistage solar still using affordable materials (Fig. 2c).

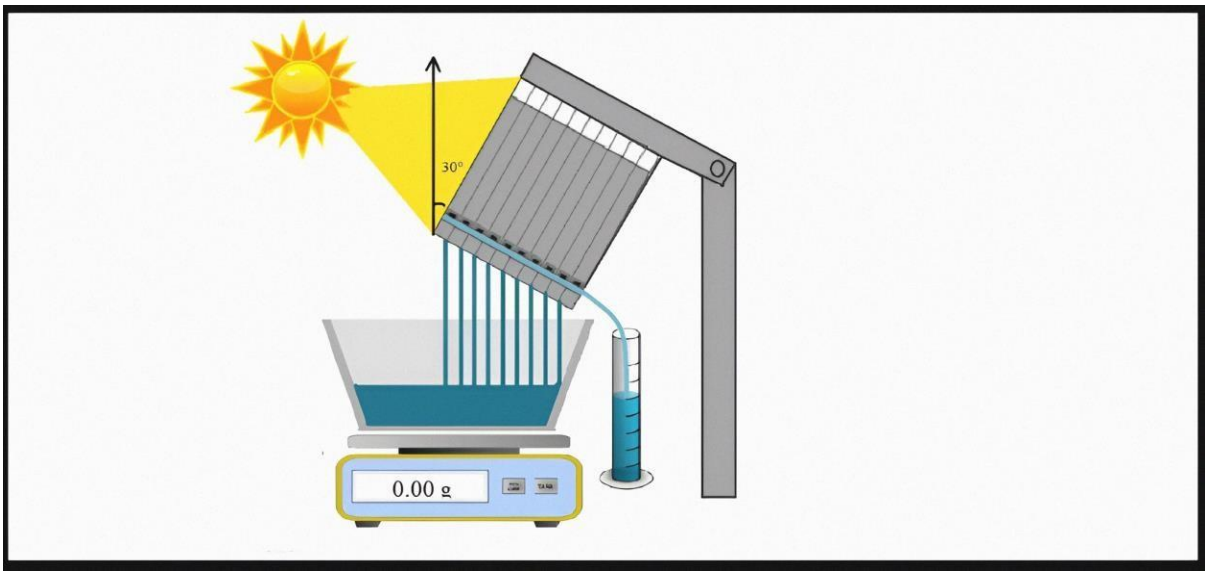

Fig. 2c Diagrammatic experimental setup

The initial stage, facing the incident sunlight, consists of a thermal insulation layer, a solar absorber, a capillary wick, and a condenser, all aligned in the direction of solar illumination. Each subsequent stage comprises a capillary wick and a condenser separated by an air gap. The condenser of the last stage is immersed in the bulk brine to maintain its temperature close to the ambient environment, ensuring a significant vapor pressure gradient across each stage.

The solar absorber, positioned between the layer and the first capillary wick, converts solar energy into heat. Thermal energy is transferred from the absorber to the capillary wick on the backside, where the brine is drawn up by capillary action and evaporates due to the elevated temperature. Vapor travels across the air gap between the evaporator and condenser, releasing thermal energy through condensation.

The condensed clean water at each stage is collected, while the released thermal energy is utilized to drive evaporation in the subsequent stage, thus achieving enthalpy recycling. The solar still architecture enables high-performance desalination by optimizing heat and mass transport through three key attributes.

Firstly, vaporization enthalpy recycling is achieved through the multistage configuration, where the latent heat from the previous stage is utilized by the next stage to induce evaporation.

3.1 MATHEMATICAL MODELLING

Upon reaching steady-state operation after 100 minutes, continuous water flow was observed from all ten outlets. We recorded a total mass loss of approximately 150 g and collected 113 g of condensed water from the ten outlets during the 3-hour test, resulting in a water collection efficiency of approximately 75%. The discrepancy between the total mass lost and collected was attributed to small droplets adhering to the condenser layers and vapor leakage during operation.

To further enhance the collection efficiency, improvements can be made in terms of increasing condenser hydrophobicity and optimizing stage sealing. By subtracting the contribution of evaporation in dark conditions from the steady-state mass loss rate (Fig. 3c), the vapor production rate of our ten-stage solar still during steady-state operation was determined to be 5.78 L/m²/h.

The solar-to-vapor conversion efficiency (Z) can be calculated based on the production rate using the equation:

$$\eta = \frac{\dot{m} h_{fg}}{q_{solar}'' A} \qquad (1)$$

where:
m represents the vapor production rate under steady state,
hfg is the enthalpy of water vaporization,
qsolar" is the input solar flux (1000 W/m²),
and A is the effective solar absorbing area.

In this study, we utilized hfg = 2394 kJ/kg, which corresponds to the latent heat at an average vapor temperature of 45°C. Sensible heat contribution was excluded from the calculation to maintain conservatism. The effective absorbing area was determined as A = 11.6 cm² based on the frame aperture size. The cumulative solar-to-vapor conversion efficiency of the ten-stage solar still prototype demonstrated in this study was 385%, aligning well with the theoretically predicted performance (417%).

To gain further insights into the heat and mass transport mechanism within the solar still, we analyzed the temperature and vapor flux at each stage during steady state (Fig. 3d). The average temperature of each stage was calculated for the last hour of the measurement period (from 120 to 180 minutes of the test). The temperature exhibited a nearly linear decline across the stages due to similar thermal resistance in each stage. To evaluate the contribution of each stage to total water production, we estimated the saturated vapor concentration based on the evaporator temperature and calculated the vapor flux using Fick's law of diffusion.

The uncertainty of vapor flux was assessed by considering temperature-induced uncertainties in mass diffusivity and vapor concentration. Vapor mass flux decreased exponentially with stage number (Fig. 3d) due to sidewall heat loss and the non-linear relationship between temperature and vapor concentration. The initial stages contributed the most to the overall efficiency, with the first three stages accounting for 45% of the total vapor flux. Optimizing the number of stages becomes crucial as the marginal benefits decrease while the material cost remains constant.

A comparison between a ten-stage and a single-stage device showed that the ten-stage device with thermal insulation achieved 385% solar-to-vapor conversion efficiency, while the single-stage device only reached 81% efficiency. Thermal design played a significant role, as removing sidewall insulation reduced the efficiency to 286%. Our ten-stage solar still prototype demonstrated a record-high solar-to-vapor conversion efficiency, outperforming previous works. Recent studies utilizing vaporization enthalpy recycling achieved improved performance, with efficiencies ranging from 72.2% to 218%. This study nearly doubled the best reported performance using unconcentrated sunlight, thanks to advanced heat and mass transfer design.

4.1 PERFORMANCE

The laboratory characterization of the solar still prototype was conducted using a solar simulator for uniform solar illumination. Twelve thermocouples were employed to monitor temperature changes in real-time, with ten of them measuring the evaporator/condenser temperatures of each stage and the remaining two recording the temperatures of the last stage's condenser and the ambient environment. Data acquisition equipment and a computer processed the temperature and mass loss data.

The transient temperature behavior of the ten stages during a 3-hour operation revealed that the first stage reached a steady state temperature of 72°C, while the subsequent stages heated gradually and also stabilized. The condenser temperature of the last stage remained slightly above the ambient temperature due to thermal resistance. The weight of the reservoir exhibited a gradual increase and eventually maintained a constant value after reaching thermal steady state. This dynamic behavior was accurately captured by a time-dependent numerical model considering temperature-dependent vapor concentration and diffusion at each stage. The condensed water started flowing from the first stage's outlet approximately 8 minutes after the solar flux was turned on, followed by the rest of the outlets.

The desalination performance of the solar still prototype was examined using simulated seawater containing 3.5 wt% NaCl. The results showed a remarkable reduction in water salinity by four orders of magnitude, surpassing the World Health Organization's drinking water standard.

To address the challenge of salt accumulation, we assessed the salt-rejection capabilities of the solar still prototype under continuous operation conditions. The first stage of the device was subjected to 1.5 sun illumination for 3.5 hours, representing a simulated day of operation. This severe condition aimed to accelerate salt accumulation and reduce diffusion time

Throughout the test, the evaporator consistently exhibited high salt-rejection capabilities. Salt accumulation was observed primarily at the two upper corners, which had the greatest diffusion resistance due to their distance from the bulk brine. Detailed analysis of one corner revealed that salt crystals began to accumulate after two hours, covering approximately 45% of the corner area after 3.5 hours. However, during the night time the accumulated salt started to diffuse back, and after 15 hours, almost all the salt returned to the bulk brine, indicating effective salt rejection.

To investigate the prototype's performance under realistic outdoor conditions, we conducted an experiment on a partly sunny day with scattered clouds. The setup was placed on a rooftop, and temperature variations in each stage were monitored using twelve thermocouples. Incident solar flux on the absorber was measured using a pyranometer, and the collected water was recorded using a camera and graduated cylinder. Despite fluctuations caused by passing clouds, the solar still prototype demonstrated a record-high outdoor productivity of 4.5-hour period. This productivity indicates the potential for utilizing 100 solar still devices in a 10x10 array to provide 10-20 L of clean water per day, depending on weather conditions.

CONCLUSION

In summary, we have developed a solar still that incorporates interfacial solar heat localization and vaporization enthalpy recycling. Our research reveals that the performance of the solar still is primarily limited by heat and mass transport within the device, which can be significantly enhanced by optimizing key factors such as the evaporator size, air gap thickness, number of stages, and sidewall thermal insulation. Following our proposed design strategy, we constructed a ten-stage solar still prototype using cost-effective materials and conducted test in outdoor settings. The results showcased a good groundbreaking solar-to-vapor conversion efficiency. We gained insights into the dynamic behavior of heat and mass transport in each stage of the system. Furthermore, we verified the solar still remarkable desalination and salt-rejection capabilities using simulated seawater. This work illustrates the potential of achieving high-performance desalination by employing a comprehensive analysis of heat and mass transport at the system level. The solar still architecture offers a practical solution for various off-grid and water-stressed regions.

ACKNOWLEDGEMENTS

Author thankful to Dr.K.Srinivas Reddy Professor, IIT Madras for helpful discussion during preparation of this manuscripts. We would like to express our sincere appreciation to Sudhish Kumar U for his invaluable guidance and support throughout this research. His insights greatly contributed to the success of this study. We are also grateful to IIT Madras for providing the necessary resources and facilities that enabled the completion of this work.

CONFLICT OF INTEREST

The authors declare no conflict of interest.

REFERENCE

1. M. M. Mekonnen and A. Y. Hoekstra, Sci. Adv., 2016, 2, e1500323.
2. J. Schewe, J. Heinke, D. Gerten, I. Haddeland, N. W. Arnell, D. B. Clark, R. Dankers, S. Eisner, B. M. Fekete, F. J. Colo´nGonza´lez, S. N. Gosling, H. Kim, X. Liu, Y. Masaki, F. T. Portmann, Y. Satoh, T. Stacke, Q. Tang, Y. Wada, D. Wisser, T. Albrecht, K. Frieler, F. Piontek, L. Warszawski and P. Kabat, Proc. Natl. Acad. Sci. U. S. A., 2014, 111, 3245–3250.
3. M. Elimelech and W. A. Phillip, Science, 2011, 333, 712–717.
4. A. D. Khawaji, I. K. Kutubkhanah and J.-M. Wie, Desalination, 2008, 221, 47–69.
5. M. Qasim, M. Badrelzaman, N. N. Darwish, N. A. Darwish and N. Hilal, Desalination, 2019, 459, 59–104.

6. A. Kabeel, Energy, 2009, 34, 1504–1509.
7. H. Ghasemi, G. Ni, A. M. Marconnet, J. Loomis, S. Yerci, N. Miljkovic and G. Chen, Nat. Commun., 2014, 5, 4449.
8. Z. Wang, Y. Liu, P. Tao, Q. Shen, N. Yi, F. Zhang, Q. Liu, C. Song, D. Zhang, W. Shang and T. Deng, Small, 2014, 10, 3234–3239.
9. K. Bae, G. Kang, S. K. Cho, W. Park, K. Kim and W. J. Padilla, Nat. Commun., 2015, 6, 10103.
10. Y. Ito, Y. Tanabe, J. Han, T. Fujita, K. Tanigaki and M. Chen, Adv. Mater., 2015, 27, 4302–4307.
11. L. Zhou, Y. Tan, D. Ji, B. Zhu, P. Zhang, J. Xu, Q. Gan, Z. Yu and J. Zhu, Sci. Adv., 2016, 2, e1501227.
12. L. Zhou, Y. Tan, J. Wang, W. Xu, Y. Yuan, W. Cai, S. Zhu and J. Zhu, Nat. Photonics, 2016, 10, 393.
13. X. Hu, W. Xu, L. Zhou, Y. Tan, Y. Wang, S. Zhu and J. Zhu, Adv. Mater., 2017, 29, 1604031.
14. C. Jia, Y. Li, Z. Yang, G. Chen, Y. Yao, F. Jiang, Y. Kuang, G. Pastel, H. Xie, B. Yang, S. Das and L. Hu, Joule, 2017, 1, 588–599. 24 H. Liu, X. Zhang, Z. Hong, Z. Pu, Q. Yao, J. Shi, G. Yang, B. Mi, B. Yang, X. Liu, H. Jiang and X. Hu, Nano Energy, 2017, 42, 115–121.
15. X. Li, X. Min, J. Li, N. Xu, P. Zhu, B. Zhu, S. Zhu and J. Zhu, Joule, 2018, 2, 2477–2484.
16. G. Xue, Q. Chen, S. Lin, J. Duan, P. Yang, K. Liu, J. Li and J. Zhou, Global Challenges, 2018, 2, 1800001.
17. E. Chiavazzo, M. Morciano, F. Viglino, M. Fasano and P. Asinari, Nat. Sustainability, 2018, 1, 763.
18. W. Wang, Y. Shi, C. Zhang, S. Hong, L. Shi, J. Chang, R. Li, Y. Jin, C. Ong, S. Zhuo and P. Wang, Nat. Commun., 2019, 10, 3012.
19. L. Zhao, B. Bhatia, S. Yang, E. Strobach, L. A. Weinstein, T. A. Cooper, G. Chen and E. N. Wang, ACS Nano, 2019, 13, 7508–7516.
20. E. Strobach, B. Bhatia, S. Yang, L. Zhao and E. N. Wang, J. Non-Cryst. Solids, 2017, 462, 72–77.
21. Y. Li, T. Gao, Z. Yang, C. Chen, W. Luo, J. Song, E. Hitz, C. Jia, Y. Zhou, B. Liu, B. Yang and L. Hu, Adv. Mater., 2017, 29, 1700981.
22. Y. Xia, Q. Hou, H. Jubaer, Y. Li, Y. Kang, S. Yuan, H. Liu, M. W. Woo, L. Zhang, L. Gao, H. Wang and X. Zhang, Energy Environ. Sci., 2019, 12, 1840–1847.
23. Y. Kuang, C. Chen, S. He, E. M. Hitz, Y. Wang, W. Gan, R. Mi and L. Hu, Adv. Mater., 2019, 1900498.
24. N. R. E. Laboratory, U.S. State Solar Resource Maps, https://www.nrel.gov/gis/solar.html, accessed 19 July, 2019.
25. M. N. Sawka, S. N. Cheuvront and R. Carter, Nutr. Rev., 2005, 63, S30–S39.